Journal of Flow Control, Measurement & Visualization, 2022, 10, 148-160
https://www.scirp.org/journal/jfcmv
ISSN Online: 2329-3330
ISSN Print: 2329-3322

An Experimental Set-Up for the *in Vitro* Simulation of a Physiological Pulsatile Flow in the Abdominal Aorta

Tiandong Lu, Jiemin Zhan, Wei Su, Wenqing Hu

Department of Applied Mechanics and Engineering, School of Aeronautics and Astronautics, Sun Yat-sen University, Guangzhou, China
Email: suwei@mail.sysu.edu.cn

How to cite this paper: Lu, T.D., Zhan, J.M., Su, W. and Hu, W.Q. (2022) An Experimental Set-Up for the *in Vitro* Simulation of a Physiological Pulsatile Flow in the Abdominal Aorta. *Journal of Flow Control, Measurement & Visualization*, **10**, 148-160.
https://doi.org/10.4236/jfcmv.2022.104009

Received: August 22, 2022
Accepted: October 25, 2022
Published: October 28, 2022

Abstract

In vitro experimental set-up is an important tool for investigating abdominal aortic aneurysm (AAA). Accurate reproduction of the physiological pulsatile flow waveform in the abdominal aorta at various anatomic locations is an important component of these experimental methods. The objective of this study is to establish an experimental set-up to generate a physiological pulsatile flow for *in vitro* simulations of the abdominal aorta. The physiological flow was established by a computer-controlled peristaltic pump and the flow field in a circular straight pipe is measured under pulsatile flow conditions by a 2-dimensional particle image velocimetry system (2D-PIV). Experimental results show that the *in vitro* experimental set-up provides a flow with a period of 2 s, a reasonable cross-sectional velocity distribution and an approximate inlet velocity profile that is close to the human abdominal aorta.

Keywords

2-Dimensional Particle Image Velocimetry System, Abdominal Aorta, Blood-Flow Experimental Set-Up, Flow Field

1. Introduction

Abdominal aortic aneurysm (AAA) is a vascular disease that leads to the arterial lumen permanently dilating to a vascular diameter of more than 1.5 times the proximal and distal normal artery diameter [1]. The global prevalence of AAA in the population aged 75 - 79 is approximately 2.4% [2]. The mortality rate following an AAA rupture is as high as 80% [3]. To date, research on the hemodynamics of AAA has mainly focused on numerical simulations and clinical re-

search. Some fundamental assumptions, such as rigid walls [4] and an ideal velocity inlet condition [5], are made to numerically simulate blood flow in the human body that compromises the reliability of the results. Although the velocity and other parameters of blood flow of patients can be obtained in clinical research studies using magnetic resonance imaging (MRI) and other equipment, it is very difficult to determine the complete flow field and more complex flow parameters. In addition, the complexity of the geometric structure of the blood system and ethical issues make it very challenging to conduct clinical research. Therefore, it is extremely important to establish an experimental set-up for generating a blood flow to study AAA haemodynamics.

Physiological pulsatile flow refers to the periodic and unsteady flow of blood through arteries at a specific frequency. Due to the complex velocity profile of physiological pulsating flow and the difficulty of performing experiments *in vitro*, many early experimental studies were conducted under steady flow conditions generated by pumps such as gear [6], submersible [7] or gravity-driven pumps [8]. However, a submersible pump generates a flow field that is considerably affected by a pressure drop and is therefore not suitable for a haemodynamic study. By contrast, a gear pump can provide a relatively stable and constant flow under a large pressure drop.

To obtain a realistic AAA flow field, it is necessary to use realistic physiological pulsatile inlet conditions (**Figure 1**). The results of experimental studies performed under steady and pulsatile inlet flow conditions show clear differences in the measured haemodynamic parameters of AAA, such that extrapolating steady flow results to some extreme conditions could result in misestimation of key parameters under physiological pulsatile flow conditions. Technological advances have produced several ways of realizing physiological pulsatile flow, including the incorporation of computer-controlled valves [9] [10], piston-cylinder combinations [11] and programmed gear pumps [12] [13] into a mock loop. The piston-cylinder combination outperforms computer-controlled valves in generating a desired flow but cannot correctly generate a physiological waveform, especially in inverse flow regions. Mechoor *et al.* developed a mock loop integrated with a feedback mechanism from the output flow to a computer-controlled gear pump system to better match the desired physiological flows and pressure waveforms, resulting in the generation of realistic physiologic flow waveforms under physiologic downstream impedances [13].

Particle image velocimetry (PIV) is a transient, multipoint, noncontact hydrodynamic velocimetry technique. There are various types of PIV, including 2D, stereoscopic, holographic and tomographic [14]. Among these PIV techniques, 2D-PIV is the most widely used and can capture a flow field illuminated by a laser to obtain two tracer particle images over small time interval. Cross-correlation calculations of tracer particle images are used to determine the quantitative velocity distribution of a cross-section of a flow field. Further processing can yield the distributions of characteristic flow-field parameters,

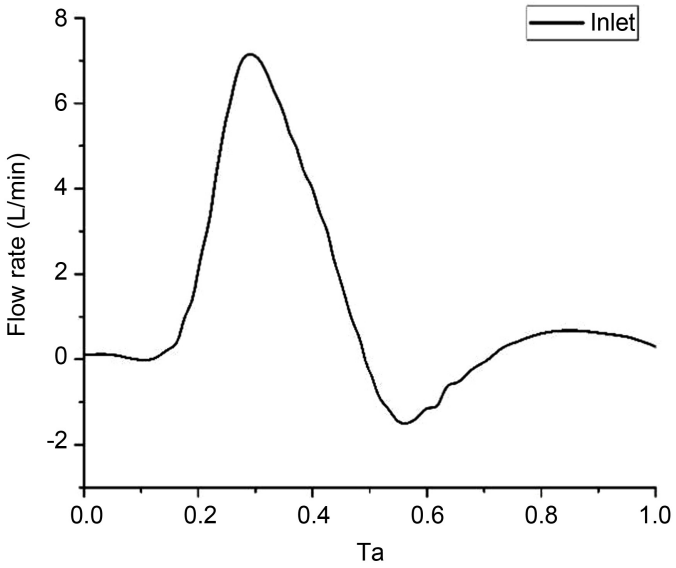

Figure 1. The *in Vivo* human flow rate derived from Olufsen *et al.* [15] by Deplano *et al.* [16].

such as the vorticity, streamlines and iso-velocity lines. Many AAA experiments have been conducted under approximate physiological pulsatile flow conditions. Yu *et al.* studied unsteady flow in a circular straight pipe and an ideal AAA model using a 2D-PIV system [17]. Deplano *et al.* used stereoscopic PIV in an *in vitro* experiment to perform a three-dimensional AAA analysis [16]. Stamatopoulos *et al.* used 2D-PIV to characterise the flow field in an axisymmetric dilated tube [8] and the velocity field in a patient-specific abdominal aneurysm model including the aorta-iliac bifurcation was measured by 2D-PIV [18]. Wang *et al.* measured the pulsating flow in a cylindrical glass tube by the Magnetic Resonance Imaging (MRI) and PIV, then results were compared to a theoretical model [19].

In this study, a physiological pulsatile flow experimental set-up is designed and built that can adjust, measure, display and record blood flow parameters. A 2D-PIV system is used to measure the flow field in a circular straight tube and obtain the cross-sectional velocity distribution and time-dependent velocity waveform; the cross-sectional velocity distribution is determined to be reasonable, thereby providing an approximation to the physiological pulsatile flow in the abdominal aorta.

2. Experimental Set-Up

Figure 2 shows the experimental section, which is connected through a flow generation device, a compliance and a rectifier plate to a circular plexiglass circular pipe that starts at the outlet of a reservoir and returns to the reservoir through a resistance at the outlet of the experimental section. The circular plexiglass pipe in the front of the experimental section has an inner diameter of 30 mm and an outer diameter of 40 mm. The pipe has a low compliance to minimize

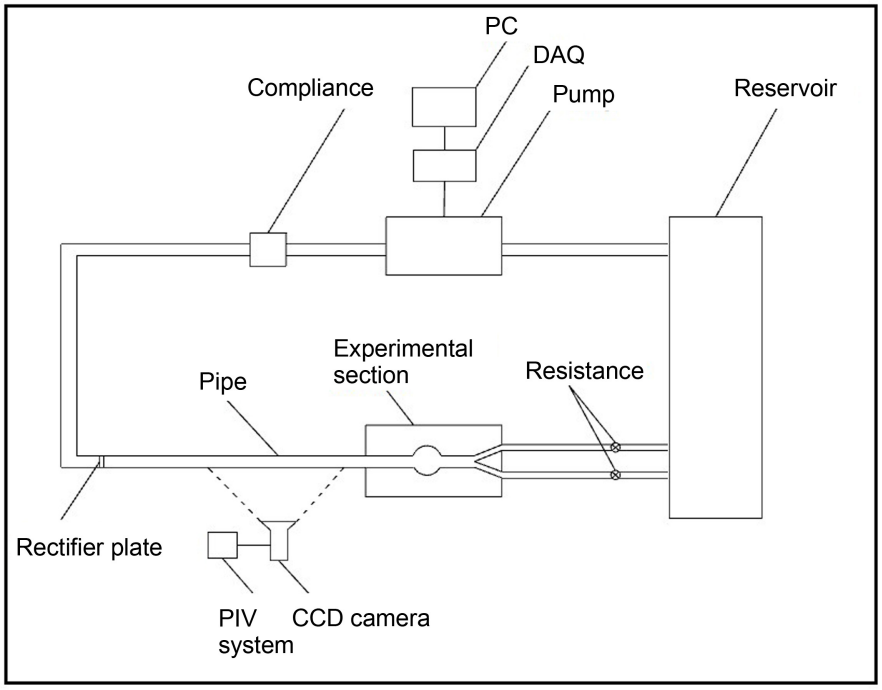

Figure 2. Schematic diagram of the physiological pulsatile flow experimental set-up.

distortion of the flow waveform and a large inner diameter to minimize flow resistance. The plexiglass circular pipe at the rear end of the experimental section has an inner diameter of 13 mm and an outer diameter of 30 mm. The two sections of the circular plexiglass pipe are connected to each other by a screw thread and to the experimental section by branch pipes. A silicone tube required for the peristaltic pump is connected to the plexiglass pipe with a special pagoda connector. The pump head tube is 25# with an inner diameter of 4.8 mm. The length of the straight plexiglass pipe at the front end of the experimental section is set to 2000 mm to ensure that the flow at the inlet of the experimental section reaches a fully developed state according to [20]

$$\frac{L}{D}=\left[0.619^{1.6}+\left(0.0567\,\mathrm{Re}\right)^{1.6}\right]^{1/1.6} \tag{1}$$

where D is the tube diameter (m), L is the entrance length (m), and Reis the Reynolds number.

A computer-controlled peristaltic pump is used to generate a physiological pulsatile flow in the experimental set-up. A glycerol-water solution with a volume ratio of 40%/60% is chosen as the working fluid. At 25˚C, the glycerol-water solution density is 1.104 kg/m^3, and its viscosity is 3.281 mPa·s, which is close to the real blood viscosity of 3.5 mPa·s. The peristaltic pump consists of a Longer L600-1FS peristaltic pump driver and a DMD15-13 pump head. The maximum rotation rate of the pump head is 600 rpm, and the rated maximum continuous output flow (25# silicone tube) is 2.07 L/min. The peristaltic pump is connected through an RS485 to the hardware of an acquisition-and-control system, which is in turn connected to an upper computer through a USB. The up-

per computer controls the pump rotation speed by sending specific voltage signals generated by the software of the acquisition-and-control system, which is independently developed in LabVIEW. The Longer DMD15-13 pump head has a unique design consisting of two groups of rollers driven by a single rotating shaft (Figure 3). The silicone tube splits into two channels at the inlet of the pump head. The output flow is extruded by two groups of rollers and combined into a single flow at the outlet of the pump head. As there is a phase difference of approximately 60˚ between the rollers in the two channels, when one side of the roller extrudes the flow in the tube, the other side does not operate; the flows of the two channels compensate each other, producing a stable flow at the pump outlet of the pump and considerably reducing the fluctuations caused by the peristaltic pump head in the flow in the mock loop.

The compliance is a flexible device that realizes force and motion transmission through elastic body deformation. A Leadfluid ZN90 compliance made of Z90-PE is used in the experimental set-up (Figure 4). The compliance is divided into upper and lower chambers. The lower chamber contains the working fluid, and the upper chamber contains air. As air is compressible and the pulse is absorbed instantaneously, a stable velocity and pressure can be achieved in the mock loop. To ensure that the fluid is reasonably distributed in the inner section of the pipe before entering the experimental section and to eliminate the influence of the pump head, pipe corner and diameter change on the flow, a rectifier plate with 35 circular holes (diameter 4.1 mm and thickness of 10 mm) is placed in the pipe at the front of the experimental section.

A NI cDAQ-9178 chassis with NI9264 and NI 9203 modules is adopted as the hardware of the acquisition-and-control system (Figure 5). The NI 9264 module sends a control voltage signal to the computer-controlled peristaltic pump to accurately adjust the pulsatile flow. A KEYENCE FD-Q20C ultrasonic flowmeter is installed outside the pipe in front of the experimental section and provides a real-time signal for the flow rate to the NI 9203 module. The ultrasonic flowmeter cannot accurately measure the flow rate and is only used during the early shakedown of the experimental set-up.

The computer software is developed in the LabVIEW environment on the Windows platform and consists mainly of modules for the control and acquisition of the flow-rate signal. LabVIEW is a graphical programming language including a front panel and a program block diagram. The operation interface of

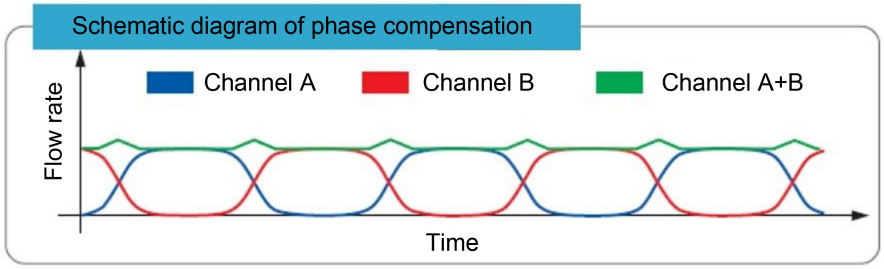

Figure 3. Schematic diagram of DMD15-13 pump head phase compensation.

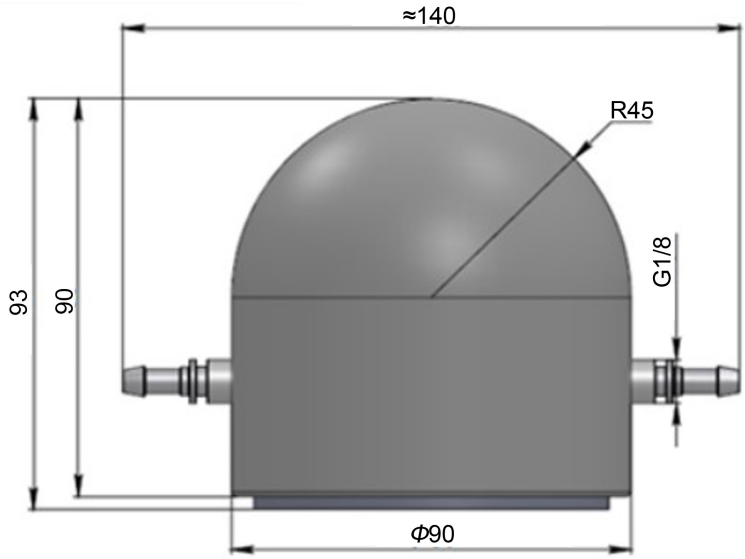

Figure 4. Diagram of the compliance.

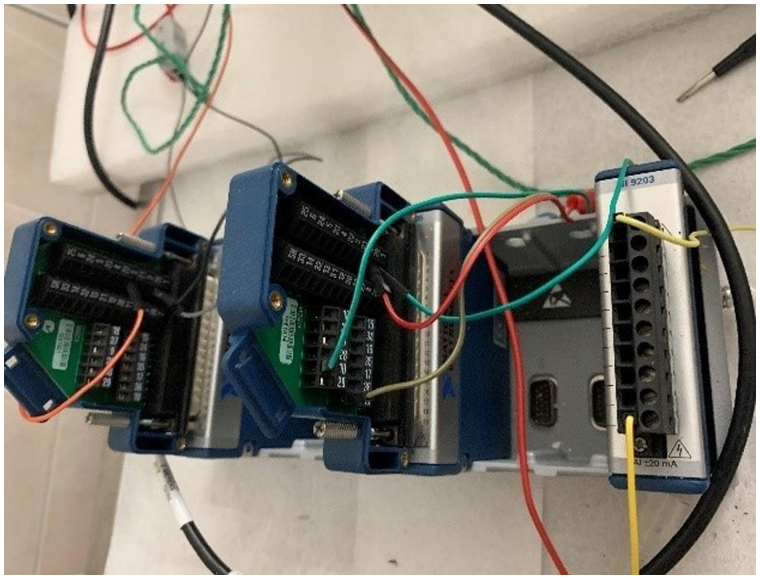

Figure 5. Hardware of acquisition-and-control system.

the virtual instruments is arranged on the front panel, and data processing, hardware data reading and control are carried out by the program block diagram. The program interface is shown in **Figure 6**.

The functions of the flow-signal control module include controlling the start and stop of the pump, adjusting the pump rotation rate, setting the control voltage gain and monitoring the control voltage signal (**Figure 7**). Digital voltage signals are converted into analogue signals to control the rotation of the pump shaft and thereby the flow rate and waveform at the outlet of the pump head. **Figure 8** shows an approximately linear relationship between the output flow and control voltage of the pump; thus, the flow rate can be controlled by adjusting the voltage gain during the experimental test.

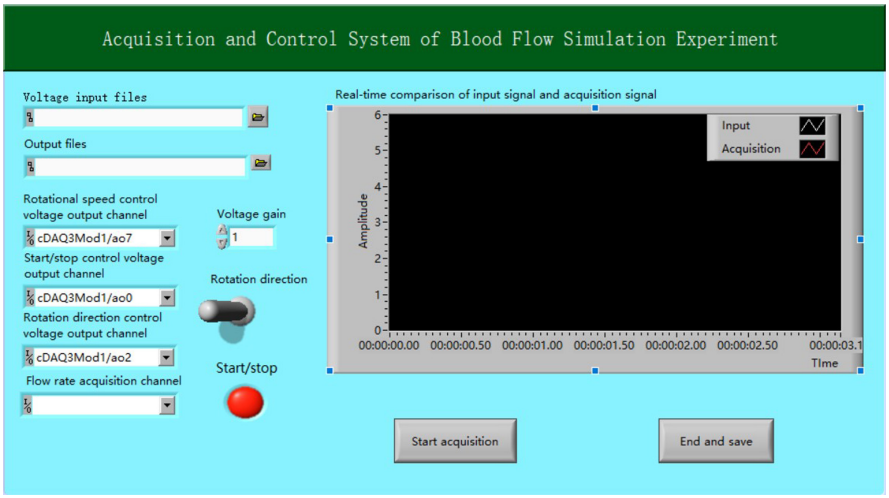

Figure 6. Acquisition-and-control system for the pulsatile flow experimental set-up.

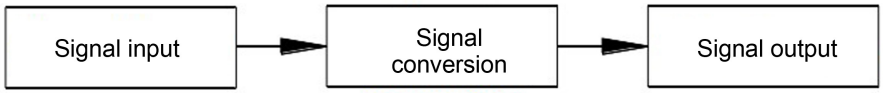

Figure 7. Flow-signal control module of the LabVIEW program.

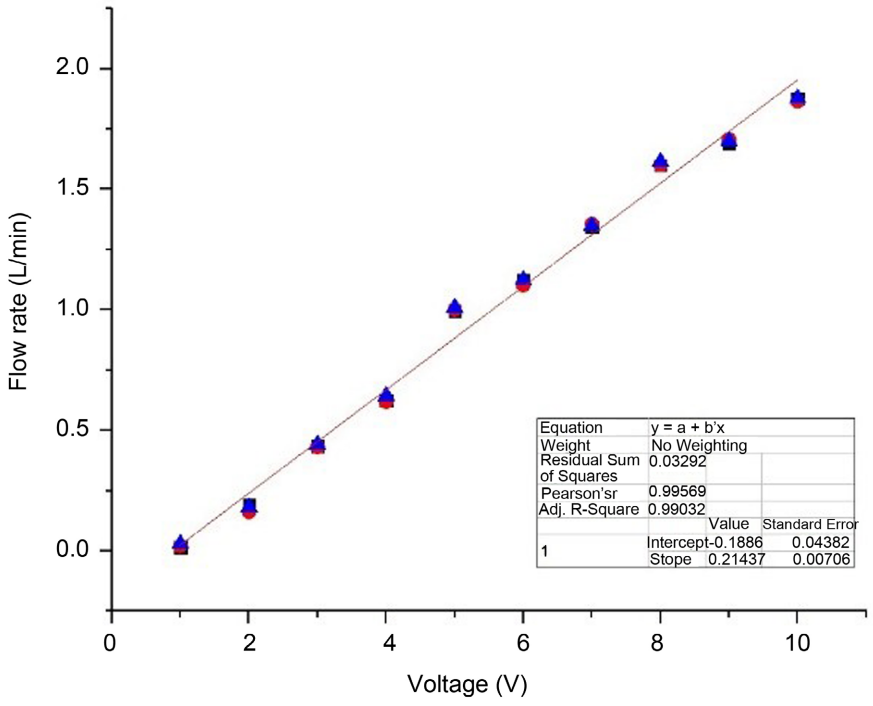

Figure 8. Relationship between control voltage and flow rate.

The functions of the flow-signal acquisition module include setting the current sampling frequency, switching the acquisition signal and real-time monitoring of the input and acquisition signal. This module collects and saves the current analogue signal of the flow sensor and synchronously adjusts the control voltage signal according to the real-time acquisition flow signal to obtain the

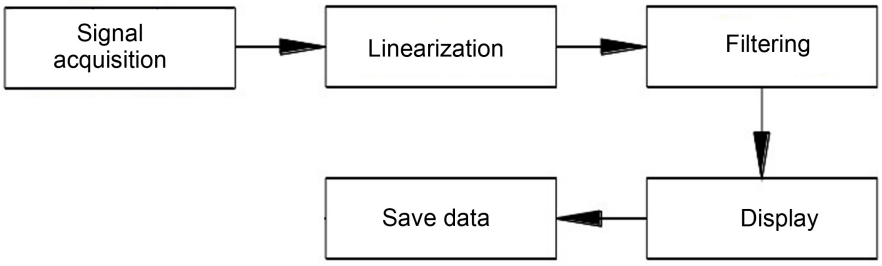

Figure 9. Flow-signal acquisition module of the LabVIEW program.

target flow waveform (**Figure 9**).

The 2D-PIV system consists of a dual-pulse solid-state laser Vlite-200 (maximum pulse energy 200 mJ and infrared wavelength 532 nm), a 5-megapixel charge-coupled device (CCD) camera and a synchronizer (**Figure 10**). Five-micrometer tracer particles are placed in the working fluid. The laser beam is expanded into a laser sheet through a combined lens to illuminate the flow field. The field of view is 100 mm by 120 mm, and Micro Vec software is used to calculate the quantitative velocity distribution of the section.

3. Results and Discussion

Investigations of the development length of laminar pipe flow have been carried out extensively and various reports of relevant work are available in the literature. According to He *et al.* [21], the maximum length of the inlet pipe to ensurefully developed flow at the model entrance under pulsating flow conditions is smaller than the inlet tube length for steady flow and for Reynolds number equal to the peak Re of the pulsating flow. According to correlations of L/D analytically for the entire Re range for laminar pipe proposed by Durst *et al.* [20], a 2000 mm long straight pipe is set in front of the inlet of the experimental section to ensure that the working fluid is fully developed when entering the experimental section.

Due to light scattering at the solid-liquid interface, a thin and bright layer form near the wall of the plexiglass circular pipe. As it is difficult to obtain the velocity distribution near the wall, the wall shear stress and the wall stress cannot be determined based on the PIV results.

The calibration curve for the pump output flow and control voltage is obtained through a series of tests. The computer is used to apply a stable integer control voltage ranging from 1 to 10 V across the peristaltic pump. The pump runs continuously for 30 s under each applied voltage, and the flow rate is measured by an ultrasonic flowmeter. The flow rate is measured three times for each applied voltage condition and averaged, and the pump output flow is related to the control voltage as follows:

The fitted relationship between the pump output flow and control voltage is as follows:

$$Q = -0.189 + 0.214U \tag{2}$$

Figure 10. Dual-pulse solid-state laser and CCD camera.

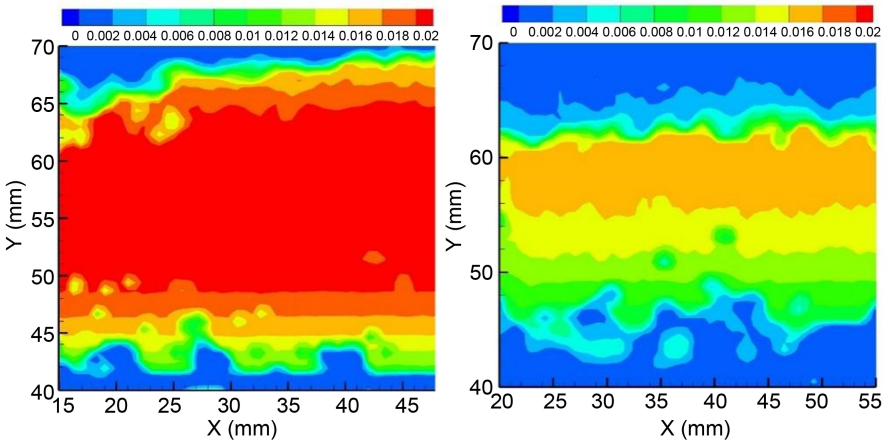

Figure 11. Contour of average velocity distribution.

where Q is the output flow and U is the control voltage.

According to the relationship between the pump output flow and control voltages, two voltage waveforms (1- and 2-s period) are used to control the pump rotation speed.

The PIV measurement section is set at the axial central longitudinal section of the straight circular pipe 200 mm in front of the experimental section. To ensure the accuracy of the measurement results, measurements are taken continuously for 30 s after the pump runs stably for 2 minutes at each working condition.

Figure 11 shows the contours of the average velocity distribution obtained over 30 s under the 1-s (left) and 2-s (right) periodic inlet conditions. Examination of the cross-sectional velocity distribution shows that the velocity is highest in the middle region and decreases towards the walls on both sides of the pipe. The maximum average velocity of the pulsating flow is approximately 0.023 m/s for the 1-s period and approximately 0.017 m/s for the 2-s period.

Figures 12(a)-(h) show the cross-sectional velocity profile at x = 20 mm during 15 - 16 s under the 1-s periodic inlet condition, and **Figures 12(i)-(p)** show the cross-sectional velocity profile section at x = 40 mm during 14 - 16 s under the 2-s periodic inlet condition. According to Stamatopoulos *et al.* and

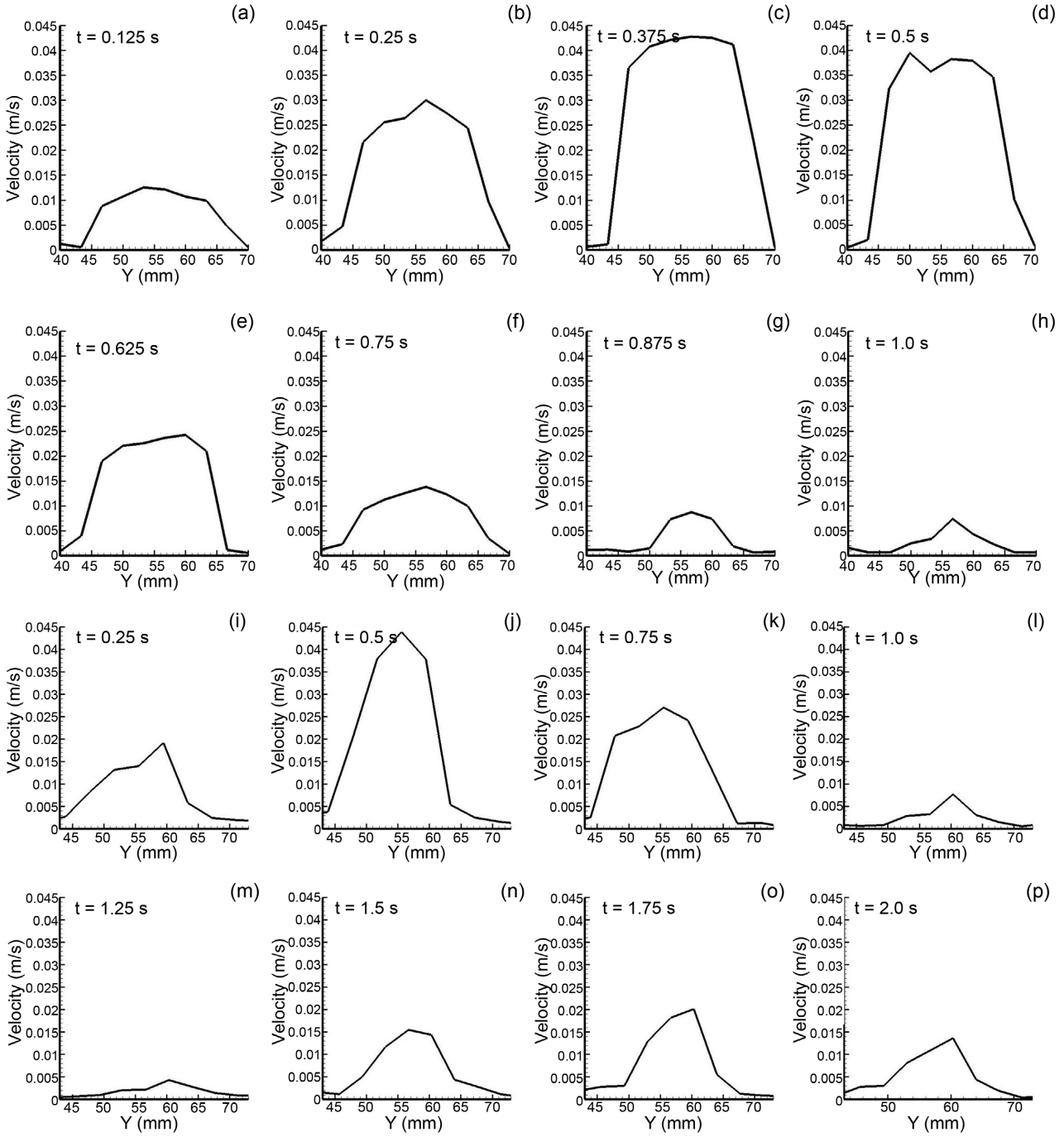

Figure 12. Cross-sectional velocity profiles at different time under 1 s (a)-(h) and 2 s (i)-(p) periodic inlet condition.

Wang *et al.* [18] [19], the form of the unsteady axial velocity profile at experimental section inlet is similar with this study. The velocity profile in the straight tube is parabolic throughout the entire cardiac cycle, which indicates that the fluid is in a fully developed state before entering the experimental section; thus, the cross-sectional velocity distribution is reasonable and meets the experimental requirements.

Figure 13(a) and **Figure 13(b)** show the velocity inlet profile obtained by

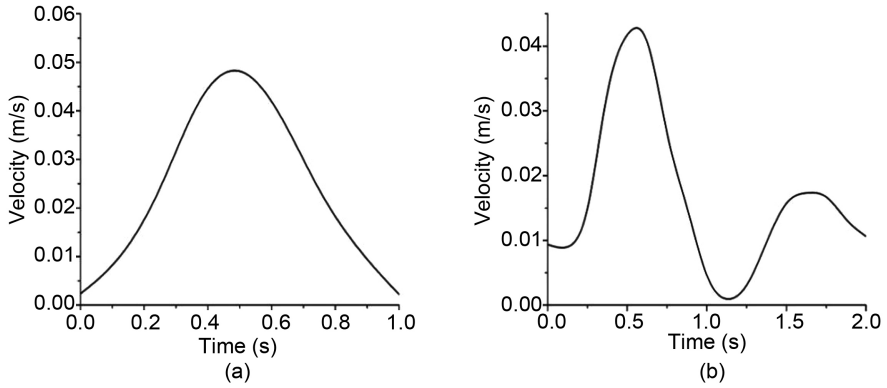

Figure 13. 1 s (a) and 2 s (b) periodic velocity profiles of the inlet of the experimental section.

integrating and averaging the cross-sectional velocity of the straight circular pipe at the entrance of the experimental section under the 1- and 2-s periodic conditions, respectively. Maximum Reynolds number of 1- and 2-s periodic flow is about 504 and 454. In the experimental study of abdominal aorta *in vitro*, the maximum velocity or waveform of the velocity inlet profile in different studies are diverse [16] [17] [18] [19], but the unified feature is clear systolic and diastolic periods. The velocity inlet profile obtained under the 2-s periodic condition has clear systolic (0 - 1.05 s) and diastolic (1.05 - 2 s) segments that are close to the entrance velocity of the human abdominal aorta. Inlet profile with clear systolic and diastolic periods could generate flow field in AAA model close to the actual flow condition, which is very important for the study of abdominal aortic aneurysm.

4. Conclusion

In this study, an experimental set-up was designed and built to generate an *in vitro* physiological pulsatile flow, for which the approximate inlet velocity profile is close to that of the human abdominal aorta. The fluid is in a fully developed state before entering the experimental section, and the velocity profile in the straight circular pipe cross-section is parabolic throughout the entire cardiac cycle, which is reasonable and meets the experimental requirements. The velocity inlet profile under a 2-s periodic inlet condition has clear systolic and diastolic segments that are similar to those of blood flow in the abdominal aorta.

Acknowledgements

This study was supported by the science and technology planning project of Guangdong province (Grant No. 2016A050502022) and the National Project of China (Grant No. 6140206040301).

Conflicts of Interest

The authors declare no conflicts of interest regarding the publication of this paper.

References

[1] Santilli, J.D. and Santilli, S.M. (1997) Diagnosis and Treatment of Abdominal Aortic Aneurysms. *American Family Physician*, **56**, 1081-1090.

[2] Sampson, U.K., Norman, P.E., Fowkes, F.G.R., Aboyans, V., Song, Y., Harrell Jr., F.E. and Murray, C. (2014) Estimation of Global and Regional Incidence and Prevalence of Abdominal Aortic Aneurysms 1990 to 2010. *Global Heart*, **9**, 159-170. https://doi.org/10.1016/j.gheart.2013.12.009

[3] Wilmink, T.B., Quick, C.R., Hubbard, C.S. and Day, N.E. (1999) The Influence of Screening on the Incidence of Ruptured Abdominal Aortic Aneurysms. *Journal of Vascular Surgery*, **30**, 203-208. https://doi.org/10.1016/S0741-5214(99)70129-1

[4] Biasetti, J., Hussain, F. and Gasser, T.C. (2011) Blood Flow and Coherent Vortices in the Normal and Aneurysmatic Aortas: A Fluid Dynamical Approach to Intra-Luminal Thrombus Formation. *Journal of the Royal Society Interface*, **8**, 1449-1461. https://doi.org/10.1098/rsif.2011.0041

[5] Cong, Y., Wang, L. and Liu, X. (2015) A Numerical Study of Fluid-Structure Coupled Effect of Abdominal Aortic Aneurysm. *Bio-Medical Materials and Engineering*, **26**, S245-S255. https://doi.org/10.3233/BME-151311

[6] Asbury, C.L., Ruberti, J.W., Bluth, E.I. and Peattie, R.A. (1995) Experimental Investigation of Steady Flow in Rigid Models of Abdominal Aortic Aneurysms. *Annals of Biomedical Engineering*, **23**, 29-39. https://doi.org/10.1007/BF02368298

[7] Antón, R., Chen, C.Y., Hung, M.Y., Finol, E.A. and Pekkan, K. (2015) Experimental and Computational Investigation of the Patient-Specific Abdominal Aortic Aneurysm Pressure Field. *Computer Methods in Biomechanics and Biomedical Engineering*, **18**, 981-992. https://doi.org/10.1080/10255842.2013.865024

[8] Stamatopoulos, C., Papaharilaou, Y., Mathioulakis, D.S. and Katsamouris, A. (2010) Steady and Unsteady Flow within an Axisymmetric Tube Dilatation. *Experimental Thermal and Fluid Science*, **34**, 915-927. https://doi.org/10.1016/j.expthermflusci.2010.02.008

[9] Moore, J.E., Ku, D.N., Zarins, C.K. and Glagov, S. (1992) Pulsatile Flow Visualization in the Abdominal Aorta under Differing Physiologic Conditions: Implications for Increased Susceptibility to Atherosclerosis. *Journal of Biomechanical Engineering*, **114**, 391-397. https://doi.org/10.1115/1.2891400

[10] Peattie, R.A., Riehle, T.J. and Bluth, E.I. (2004) Pulsatile Flow in Fusiform Models of Ab dominal Aortic Aneurysms: Flow Fields, Velocity Patterns and Flow-Induced Wall Stresses. *Journal of Biomechanical Engineering*, **126**, 438-446. https://doi.org/10.1115/1.1784478

[11] Tsai, W. and Savaş, Ö. (2010) Flow Pumping System for Physiological Waveforms. *Medical & Biological Engineering & Computing*, **48**, 197-201. https://doi.org/10.1007/s11517-009-0573-6

[12] Deplano, V., Knapp, Y., Bailly, L. and Bertrand, E. (2014) Flow of A Blood Analogue Fluid in A Compliant Abdominal Aortic Aneurysm Model: Experimental Modelling. *Journal of Biomechanics*, **47**, 1262-1269. https://doi.org/10.1016/j.jbiomech.2014.02.026

[13] Mechoor, R.R., Schmidt, T. and Kung, E. (2016) A Real-Time Programmable Pulsatile Flow Pump for *in Vitro* Cardiovascular Experimentation. *Journal of Biomechanical Engineering*, **138**, Article ID: 111002. https://doi.org/10.1115/1.4034561

[14] Roloff, C., Stucht, D., Beuing, O. and Berg, P. (2019) Comparison of Intracranial Aneurysm Flow Quantification Techniques: Standard PIVvs Stereoscopic PIVvs

Tomographic PIVvs Phase-Contrast MRIvs CFD. *Journal of Neurointerventional Surgery*, **11**, 275-282. https://doi.org/10.1136/neurintsurg-2018-013921

[15] Olufsen, M.S., Peskin, C.S., Kim, W.Y., Pedersen, E.M., Nadim, A. and Larsen, J. (2000) Numerical Simulation and Experimental Validation of Blood flow in Arteries with Structured-Tree Outflow Conditions. *Annals of Biomedical Engineering*, **28**, 1281-1299. https://doi.org/10.1114/1.1326031

[16] Deplano, V., Guivier-Curien, C. and Bertrand, E. (2016) 3D Analysis of Vortical Structures in an Abdominal Aortic Aneurysm by Stereoscopic PIV. *Experiments in Fluids*, **57**, Article No. 167. https://doi.org/10.1007/s00348-016-2263-0

[17] Yu, S.C.M. (2000) Steady and Pulsatile Flow Studies in Abdominal Aortic Aneurysm Models Using Particle Image Velocimetry. *International Journal of Heat and Fluid Flow*, **21**, 74-83. https://doi.org/10.1016/S0142-727X(99)00058-2

[18] Stamatopoulos, C., Mathioulakis, D.S., Papaharilaou, Y. and Katsamouris, A. (2011) Experimental Unsteady Flow Study in a Patient-Specific Abdominal Aortic Aneurysm Model. *Experiments in Fluids*, **50**, 1695-1709. https://doi.org/10.1007/s00348-010-1034-6

[19] Wang, Y., Joannic, D., Patrick, J., Keromnes, A., Aurélien, M., Lalande, A. and Fontaine, J.F. (2016) Comparison of Flow Measurement by 4D Flow Magnetic Resonance Imaging and by Particles Image Velocimetry on Phantom of Abdominal Aortic Aneurysm. *SM Vascular Medicine*, **1**, Article No.1008.

[20] Durst, F., Ray, S., Ünsal, B. and Bayoumi, O.A. (2005) The Development Lengths of Laminar Pipe and Channel Flows. *Journal of Fluids Engineering,* **127**, 1154-1160. https://doi.org/10.1115/1.2063088

[21] He, X. and Ku, D.N. (1994) Unsteady Entrance Flow Development in a Straight Tube. *Journal of Biomechanical Engineering*, **116**, 355-360. https://doi.org/10.1115/1.2895742